Experimental and numerical study of mixing characteristics of a rectangular lobed mixer in supersonic flow

J.-H. Feng
564771857@163.com
C.-B. Shen
cbshen@nudt.edu.cn
Q.-C. Wang and J. Lei
Science and Technology on Scramjet Laboratory
College of Aerospace Science and Engineering
National University of Defense Technology
Changsha
China

ABSTRACT

A combined experimental and computational study on a rectangular lobed mixer is performed. A series of simulations based on a steady Reynolds-averaged Navier-Stokes Simulation (RANS) are conducted to analyse the mixing mechanisms of large-scale streamwise structure shed by the trailing edge of lobed mixer, with emphasis being placed on the effect of turbulence modeling and inflow conditions. The simulations are validated in respect of velocity and scalar distribution against the data obtained through Particle Image Velocimetry (PIV) and Nanoparticle-based Planar Laser Scattering (NPLS) technique. The computational results predicted by the SST k–ω turbulence model show better agreement with the experimental data. But the small-scale turbulence structures are not captured accurately by these turbulence models. The convoluted shear layer shed from trailing edge is stretched and rotated by the large-scale streamwise vortices, forming an unstable 'pinching-off' structure, which increases the interfacial area. And at the interface of two streams, a large number of small-scale turbulence structures are formed, which contribute a lot to the mixing enhancement along with the increased interfacial area. The streamwise vorticity decays more rapidly with the decrease of velocity ratio and total pressure ratio of two streams. The scalar thickness which reflects the mixing rate of two streams increases with the decreasing velocity ratio and total pressure ratio.

Paper No. 4209. Manuscript received 28 May 2014, revised version received 12 October 2014, accepted 18 November 2014.

https://doi.org/10.1017/S0001924000010782 Published online by Cambridge University Press

NOMENCLATURE

A cross-section area (m^2)
a_1 sound speed of upper stream (ms^{-1})
a_2 sound speed of lower stream (ms^{-1})
h height of the lobe (m)
M_c convective Mach number
P_o total pressure (KPa)
P_{o1} total pressure of upper stream (KPa)
P_{o2} total pressure of lower stream (KPa)
r velocity ratio
Re_λ characteristic Reynolds number
s density ratio
T_o total temperature (K)
tp total pressure ratio
U streamwise velocity (ms^{-1})
U_1 upper stream velocity (ms^{-1})
U_2 lower stream velocity (ms^{-1})
U_a averaged streamwise velocity (ms^{-1}), $(U_1 + U_2)/2$
V transverse velocity (ms^{-1})
W spanwise velocity (ms^{-1})
α penetration angle of the lobe
δ scalar thickness
ω normalised streamwise vorticity
Γ streamwise circulation
Γ^* normalised streamwise circulation

SUBSCRIPTS

1 upper stream
2 lower stream
x streamwise direction
z spanwise direction
y transverse direction

1.0 INTRODUCTION

The air-breathing combined cycle propulsion system is believed to be the next-generation booster for potential launch vehicles access to orbit. One important aspect related to this system is the efficient fuel-air mixing system. Due to the extreme short residence time, a rapid mixing between the supersonic/high subsonic fuel jet (or fuel-rich stream) and the intake air is desired. The conventional gradient-type mixing mechanism is less efficient for the rapid decrese of the growth rate of mixing layer with the increase of convective Mach number in compressible fluid[1-2]. Hence, novel methods to enhance mixing have to be proposed. A comprehensive review related to the techniques of enhancing mixing in compressible flow was summarised by Gutmark[3] and Seiner[4]. It is widely accepted that the introducing large-scale streamwise vortices into the flow field are an attractive method for mixing enhancement, and the lobed mixer has been considered effective in generating large-scale streamwise vortices. The most widely application of the lobed

https://doi.org/10.1017/S0001924000010782 Published online by Cambridge University Press

mixer is in the exhaust systems of turbofan engines for nozzle noise reduction[5-8], as well as for thrust augmentation and infrared radiation suppression in ejector systems[9-11]. Recently, the mixers are widely exploited in the combustion of scramjets, referred to as the petal nozzles[12,13] or lobed injectors[14-16], to improve the molecular mixing of chemical species.

The schematic of a classic lobed mixer and the generated vortical structures formed downstream of its trailing edge are shown in Fig. 1. These vortical structures were firstly explained by McCormick and Bennett[17]. The Kevin-Helmholtz (K-H) vortices are generated as a result of the inviscid instability of the inflectional mean axial velocity profile (K-H instability) of the free shear layer between two co-flowing streams[18-19]. These structures are a fundamental mechanism that yields mass and momentum exchange. The streamwise vortices reproduced by the trailing edge of lobes that alternately turns the two streams into the troughs of the lobes are believed to be primarily responsible for the enhanced mixing. Paterson[7,20] was the first to realise the streamwise vortices created from the radially oriented secondary flows also enhanced mixing significantly in additioin to the increased interfacial area. Subsequent studies by Werle *et al*[21] and Eckerle *et al*[22] revealed that the vortex formation of secondary flows was an inviscid process and the magnitude of these vortices was dependent on both the lobe shape and the penetration angle. Manning[19] and Elliott *et al*[23] proposed that the breakdown of K-H vortices due to the interaction of the K-H vortices and the streamwise vortices contribute to the mixing. McCormick and Bennett[17] further investigated experimentally the mixing mechanism downstream of the lobed mixer in detail and concluded that the intense small-scale turbulence mixing was mainly due to the formation of the pinched-off structures which is unstable. Similar conclusions were obtained by the Belovich *et al*[24], Hu *et al*[25-28] and Yu *et al*[29]. More recently, the K-H vortex rolling-up mechanisms in the enhanced mixing processes has been partly revealed[30-34]. Notably, Nastase, *et al*[32,33] found out a transverse shear induced by the lobes leaded to a breakdown of the K-H structure into 'ring segments' due to the strong variation of the exit plane curvature, and they suggested that the entrainment rate increased as to the streamwise structure was not attenuated by their roll up due to the discontinuous nature of the K-H vortices. Finally, the small-scale horseshoe vortices existing within the troughs of the lobes are also commonly observed downstream of the trailing edge[17,25], which have been proved to impose little impact on the overall mixing process.

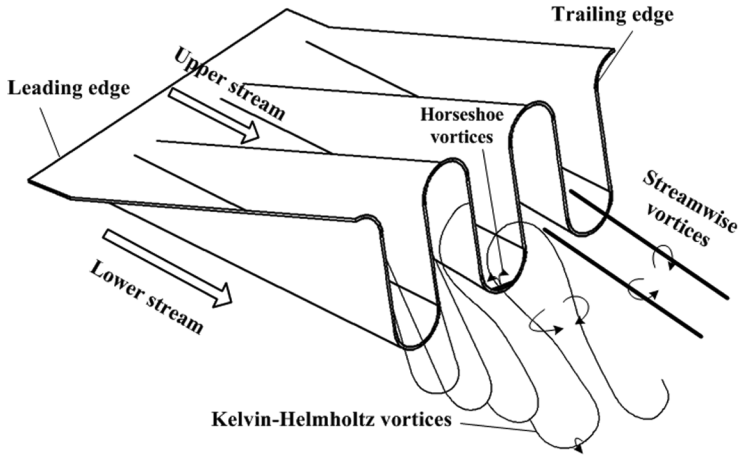


Figure 1. Generic lobed mixer contours and schematic of the main vortical structures (adapted from McCormick and Bennett[17]).

https://doi.org/10.1017/S0001924000010782 Published online by Cambridge University Press

Elliott, *et al*[23] and Waitz, *et al*[35] extended the study of lobed mixers to the compressible flow, showing that the compressibility had a marginal influence on the generation and the evolution of the streamwise vortices, since it was believed that the radially oriented secondary flow developed by the side walls of the lobes was incompressible and non-viscous. Tew[36,37] concluded that the compressibility had twofold effects on the mixing dominated by streamwise vortices. One was that the streamwise vorticity had more time to stretch the interface between the two streams because of the reduced shear growth rate associated with high convective Mach number; the other was that the interaction of trailing-edge shocks and density gradients across the mixing layer may generate additional streamwise vortices, which is referred as the baroclinic effect.

In addition, several numerical studies have been performed to study the three-dimensional flow field downstream of the lobed mixer. Originally, a steady RANS approach in conjunction with a turbulence model[38-42] and a vortex-element approach[43] were used to calculate lobed mixer flows, and the effect of boundary conditions on the numerical results were also considered in these studies[39-41]. Subsequent studies with regard to mixing characteristics of lobes have simulated multiple or realistic lobed nozzles using a large-eddy simulation (LES) approach[44,45]. More recently, Brinkerhoff, *et al*[46] investigated the mixing mechanisms downstream of an axisymmetric lobed mixer using an unsteady RANS approach, showing the transient behaviour of the lobed-mixer flow. The K-H vortices, streamwise vortices and their mutual interactions were analysed.

Although many important results have been obtained through these experimental and computational investigations, the mixing mechanisms of lobed-mixer flows are not clearly uncovered. Most of the efforts are devoted to the incompressible flow downstream of the lobed mixer, while seldom has the work been done to address the compressible case. Though Waitz, *et al*[35] and Tew[36,37] have investigated the mixing characteristics in compressible regimes, their work was confined to the effect of compressibility on the mixing process with existence of streamwise vortices, while the detailed mixing mechanisms in supersonic regimes are not presented. Besides, the computational studies that have been performed regarding the three-dimensional supersonic flow field downstream of the lobed mixer are limited. Georgiadis *et al*[42] investigated turbulence modeling effects on the prediction of lobed nozzle flow fields, but they have just calculated the subsonic lobed flow fields and not extended these simulations to the supersonic regime. The present study attempts to investigate the development of supersonic flow downstream of the lobed mixer using a combined experimental and computational method. One objective of present work is to perform a detailed quantitative comparative study of velocity and scalar distribution of different turbulence models to evaluate the prediction capability of turbulence models for the supersonic lobed flow fields. Another one is to discuss and identify the effect of inflow parameters on the supersonic streamwise vortices to analyse the sensitivity of the mixing characteristics to the inflow parameters.

2.0 EXPERIMENTAL APPROACHES

2.1 Experimental installation

The experiment is conducted in the supersonic mixing layer wind-tunnel at the Science and Technology on Scramjet Laboratory, National University of Defense Technology (NUDT). This wind tunnel which is suction type consists of separate settling chambers, a double supersonic nozzle, a test section and other auxiliary equipment, as shown in Fig. 2. Air as the inflow is

https://doi.org/10.1017/S0001924000010782 Published online by Cambridge University Press

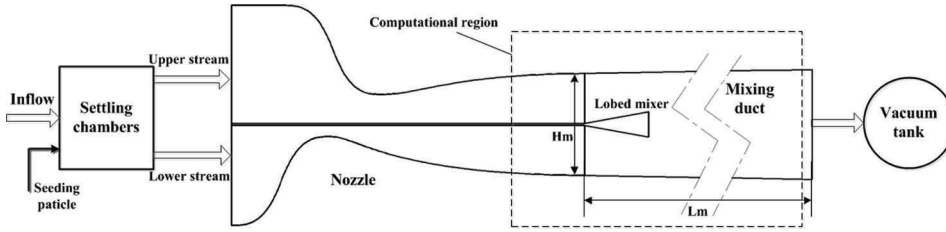


Figure 2. The experimental setup.

breathed in the wind tunnel since the pressure difference between the environment and vacuum tank. The settling chambers separated by a flat splitter are designed to ensure uniform and low noise flow at the entrance of the test section. The total pressure can be adjusted by the pressure controller to realise pressure matching between the two streams. The lobed mixer placed at the trailing of the flat splitter. The test section, also named mixing duct, is 350in length, 60in height and 200in width, and the optics windows are equipped on four sides of the duct. To eliminate the streamwise pressure gradient, the upper and lower walls are diverged by 0·5°. In present experiment, the calibrated Mach numbers of nozzle exit are 2·1 and 3·3 for the upper and lower streams respectively. Other relevant measured parameters are shown in Table 1.

Table 1
Experimental parameters of supersonic mixing layer wind tunnel

Property	Upper stream	Lower stream
Ma	2·1	3·3
P_0(KPa)	18·8	101·0
T_0(K)	300·0	300·0
U (ms^{-1})	532·9	646·8
Mc	0·25	
Re_λ	$1{\cdot}13 \times 10^5$	

2.2 The NPLS and PIV technique

The NPLS experiment system developed by Zhao, *et al*[47] is used to obtain instantaneous flow visualisation. This setup is composed of a tracer generation, a synchronisation system, a recording system, a light source and a post-processing system. The operating principle of this system is described in detail in Refs 48-49. It has been proved effective in capturing the supersonic fine vortical structures[50,51]. The NPLS system is used to obtain the streamwise/spanwise vortices structure downstream of lobed mixers. TiO_2 nano-particles with diameters of 42·5nm are selected as tracers, and a double-pulsed Nd: YAG laser, with wavelength of 532mn, pulse energy of 350mj per 6ns is used to illuminate the flow region of interest. The CCD camera with resolution of 4,096 × 2,600 pixels can provide a maximum spatial resolution of 10μ*m*/pixels. The PIV shares the same control system with the NPLS.

https://doi.org/10.1017/S0001924000010782 Published online by Cambridge University Press

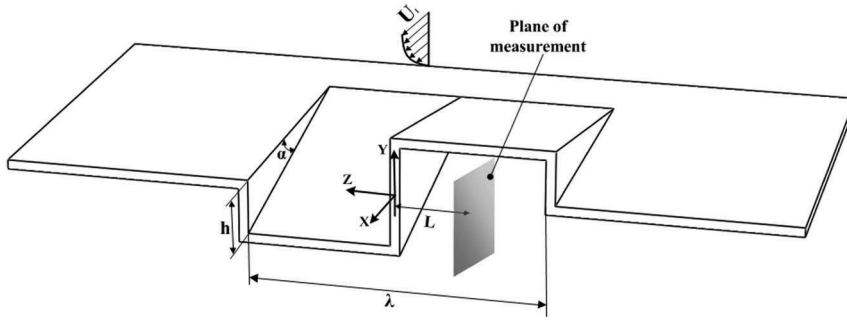


Figure 3. Geometry and Cartesian-co-ordinate system of the lobed mixer.

2.3 Mixer configuration

Details of mixer configuration studied are shown in Fig. 3. Important parameters which define a lobed mixer are the lobe wavelength ($\lambda = 31$mm), the lobe height ($h = 5{\cdot}8$mm) and the penetration angle ($\alpha = 15^{o}$). The height to wavelength ratio (h/λ) is 0·2, and the trailing-edge thickness is 1mm. Fig. 3 also shows the positions of measuring plane in the Cartesian co-ordinate system. Six *X*-*Y* planes ($Z = \pm 0{\cdot}15\lambda$, $Z = \pm 0{\cdot}28\lambda$ and $Z = \pm 0{\cdot}42\lambda$) are measured using the PIV technique, and three *Y*-*Z* planes ($x = (1/3)\lambda$, $x = (4/3)\lambda$ and $x = (7/3)\lambda$) are surveyed qualitatively employing the NPLS method.

3.0 MATHEMATICAL MODELS

3.1 Mathematical model

The numerical results are obtained through solving the full 3D form of the Navier-Stokes (N-S) equations in Favre-averaged form for compressible steady flows. Using Cartesian tensor notation they may be written as:

Continuity equation

$$\frac{\partial}{\partial x_i}(\rho u_i) = 0 \qquad \ldots (1)$$

Equation of conservation of momentum

$$\frac{\partial}{\partial x_j}(\rho u_i u_j) = -\frac{\partial p}{\partial x_i} + \frac{\partial \tau_{ij}}{\partial x_j} + \frac{\partial}{\partial x_j}(-\overline{\rho u_i' u_j'}) \qquad \ldots (2)$$

Equation of conservation of energy

$$\frac{\partial}{\partial x_j}(\rho H u_j) = -\frac{\partial q_j}{\partial x_j} + \frac{\partial \tau_{ij} u_i}{\partial x_j} + \frac{\partial}{\partial x_j}(-\overline{\rho u_i' u_j' u_i}) + \frac{\partial}{\partial x_j}(-\overline{\rho H' u_j'}) \qquad \ldots (3)$$

Where

$$\tau_{ij} = \mu\left(\frac{\partial u_i}{\partial x_j} + \frac{\partial u_j}{\partial x_i}\right) - \frac{2}{3}\mu \frac{\partial u_k}{\partial x_k}\delta_{ij} \qquad \ldots (4)$$

https://doi.org/10.1017/S0001924000010782 Published online by Cambridge University Press

And:

$$q_i = -\kappa \frac{\partial T}{\partial x_i} \quad \ldots (5)$$

$$p = \rho RT = (\gamma - 1)\rho(E - \frac{1}{2}u_i u_i) \quad \ldots (6)$$

The effect of body forces is neglected in these equations and the viscosity μ is solved according to the Sutherland's law. The ratio of specific heat γ and thermal conductivity κ are viewed as the constants. Density ρ and pressure p are Reynolds-averaged properties, whereas velocity component u_i, inner energy E, enthalpy H and temperature T are density-weighted Favre-averaged properties. The Reynolds stresses, $-\rho\overline{u_i' u_j'}$ must be modeled in order to close the Equation (2). A common method based on the Boussinesq hypothesis correlates the Reynolds stresses with the mean velocity gradients:

$$-\overline{\rho u_i' u_j'} = \mu_t(\frac{\partial u_i}{\partial x_j} + \frac{\partial u_j}{\partial x_i}) - \frac{2}{3}(\rho k + \mu_t \frac{\partial u_k}{\partial x_k})\delta_{ij} \quad \ldots (7)$$

The Boussinesq hypothesis is used in the Spalart-Allmaras model, the $k-\varepsilon$ model, and the $k-\omega$ model. The detailed specification about these models is given in the Ref. 51. In order to assess the applicability of the seven turbulent models to lobed mixer flows and choose a turbulence model that has a good prediction as to subsequent numerical studies, seven turbulence models based on the Boussinesq hypothesis are employed to calculate the three-dimensional supersonic flowfields downstream of the lobed mixer.

3.2 Numerical method

The solution of the above governing equations together with the turbulence model equations are obtained with density-based (coupled) steady solver of FLUENT [51]. The second order spatially upwind scheme with the advection upstream splitting method (AUSM) flux vector splitting is utilised.The entire computational domain extended 2·5 lobe wavelengths upstream and 4 lobe wavelengths downstream of the mixer trailing edge is shown in Fig. 2, and the height of computational domain is identical with that of wind tunnel. At the inflow, the total/static pressure and the total temperature are imposed, and the turbulent intensity is specified 1% according to the experimental conditions, whereas all the physical variables are extrapolated from the internal domain due to the supersonic flow at the outflow. The no-slip conditions are assumed for the walls, and the near-wall region flow is modeled adopting the standard wall functions. In order to visualise the scalar mixing fraction of the two streams from upper and lower channel, a mixture model included two components (one inlet stream is assigned a scalar value of 1, while the other is set to 0) is introduced in this simulation, and the air is assumed to be a calorifically perfect gas. The criterion for convergence is that the residuals do not change after falling for more than four orders of magnitude and the difference between the inflow and outflow mass flux is exhibited to drop below 1×10^{-3}kg/s.

A hybrid grid generated using the commercial software Gambit, and the computational domain is multi-blocked for the purpose of controlling the grid quality. Figure 4 shows the entire grid for the computational domain and the partial grid near the mixer. It is clearly demonstrated that the unstructured tetrahedral gird is generated in the vicinity of mixer in order to minimise skewness, and a size function is utilised to cluster the grid around the mixer. However, the mixing duct is structured to maximise grid orthogonality, and denser grid is designed in the mixing layers to

https://doi.org/10.1017/S0001924000010782 Published online by Cambridge University Press

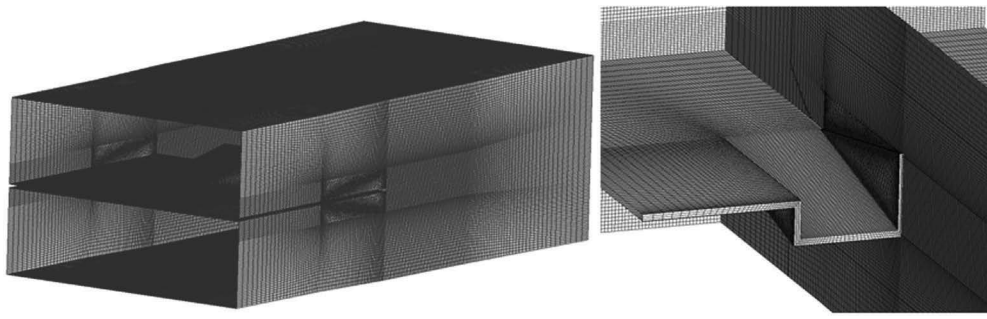


Figure 4. Schematic of a typical grid system employed. (a) Entire grid, (b) A close-up view.

resolve the complex vortex structure. Furthermore, the grid spacing at the wall is set to 0·06mm, which insures the smallest value of y^+ in the whole computational domain is limited in the range of 30-100 which is located in the log-law layer. In order to analyse the grid independency in this numerical process, three sets of mesh with different number of cells, namely approximately 1·22million, 2·24 million and 3·27 million, have been performed.

4.0 RESULT AND DISCUSSION

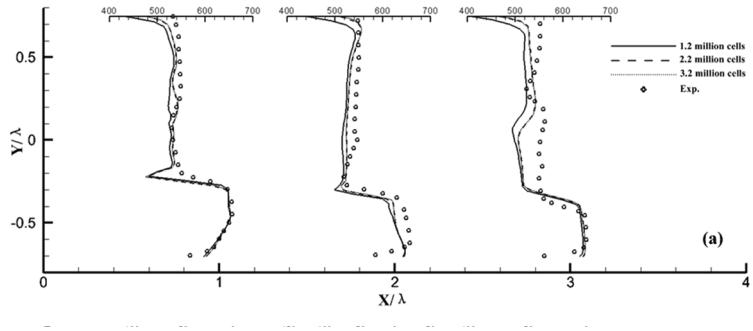
4.1 Grid independence analysis and numerical validation

Typical streamwise and transverse velocity profiles at different positions ($X = \lambda$, $X = 2\lambda$ and $X = 3\lambda$) downstream of the trailing edge with different grid scales are shown in Fig. 5. The averaged velocity data obtained from the PIV measurement is also shown in Fig. 5, and the uncertainty in the measure velocity is more or less 1·5%. The SST $k-\omega$ turbulence model is used initially in this paper to validate the grid impendency since this model is believed to be able to describe the mixing process developed by the lobed mixer in compressible flow[42]. The predicted results obtained by grid of 2·2 million and 3·2 million show better agreement with the experimental data than those with the coarse grid of 1·2 million. It is obvious that the streamwise velocities (U-velocities) in the near field of the lobes are predicted well with all grid scales, and the transverse velocities (V-velocities) with all grid scales makes only a slight difference in the near field of lobes. However, in the farfield downstream of trailing edge, the predicted results of U-velocities and V-velocities do not match accurately with the experimental data. These differences are attributed to the turbulent model effect and will be analysed in the next content. However, the numerical approach used here can capture the trend of the measured profiles with a slight offset in the near field of lobed flow. Moreover, it is also observed that the case with grid of 2·2 million differs little from that of 3·2 million, suggesting that the grid of 2·2 million is capable of predicting the flow. Therefore, the grid scale with 2·2 million cells is chosen.

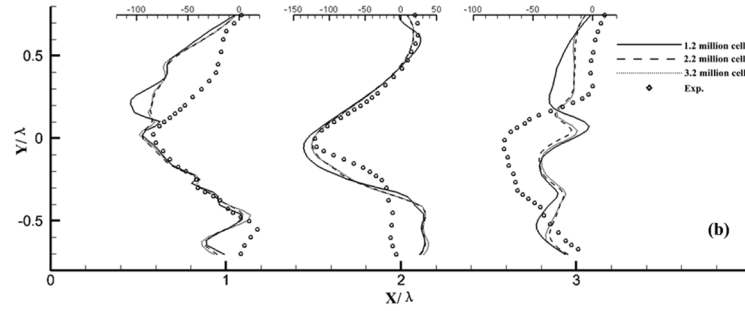
4.2 Turbulence model analysis

The main flow features of lobed mixer in compressible flow are the oblique shock and large-scale vortices structures, which should be captured for an accurate simulation. Two types of oblique shock are expected, one is the leading shock generated at the leading edge and the other one is the

https://doi.org/10.1017/S0001924000010782 Published online by Cambridge University Press



(a)



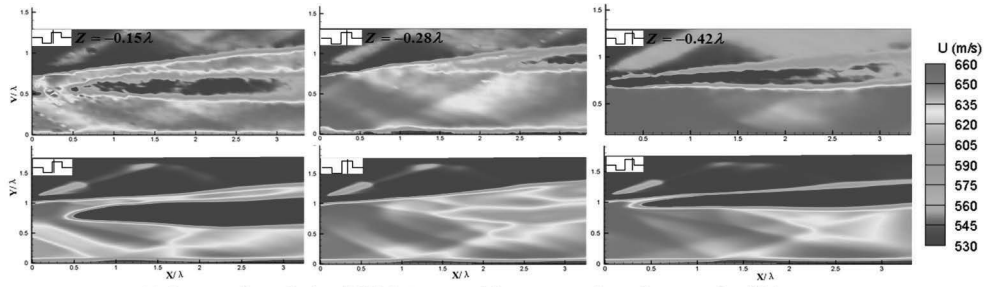
(b)

Figure 5. Comparison of the velocity profiles for different grid scales at different position downstream of the trailing edge at the measure plane of L = 0·28λ. (a) The U-velocity, (b) The V-velocity.

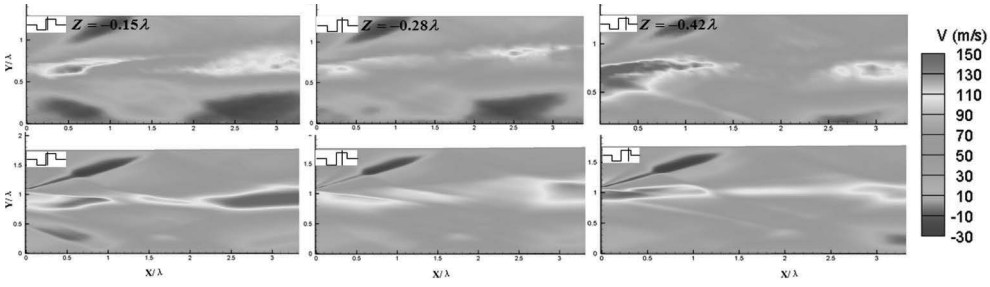
trailing shock generated owing to the unmatched pressure of two streams downstream the trailing edge. A qualitative and quantitative comparison of the numerical results acquired from seven turbulence models with the experimental data is performed to evaluate the effect of turbulence modeling on the prediction.

Figure 6 shows the comparison of streamwise and transverse velocity contours between the experimental data and computed results at the peak region (three measurement plane of Z = –0·15λ, Z = –0·28λ and Z = –0·42λ), and the streamwise and transverse velocity contours at the trough region (three measurement plates of Z = 0·15λ, Z = 0·28λ and Z = 0·42λ) are shown in Fig. 7. It is obvious that the numerical results obtained by the SST k – ω turbulent model show good agreement with the experimental data except for the plane of Z = 0·15λ at the trough region. The PIV data from the plate of Z = 0·15λ is untrue in the near field downstream of the trailing edge due to the inadequate particle quantity. The primary features of supersonic lobed flow, including the leading and trailing shock and the cross-section secondary flow induced by the streamwise vortices, are well captured by the SST k – ω turbulent model. Higher entrainment is achieved attribute to the combined effects of the streamwise vortices and shock structure compared with traditional planner mixing layer. Furthermore, the transverse velocity is also larger due to the cross-section secondary flow induced by the streamwise vortices. Hence, it is suggested that the streamwise vortices generated by the lobed mixer increase the entrainment rate of the lobed mixing layer, thereby leading to the increase in mixing rate of the supersonic lobed flow.

https://doi.org/10.1017/S0001924000010782 Published online by Cambridge University Press

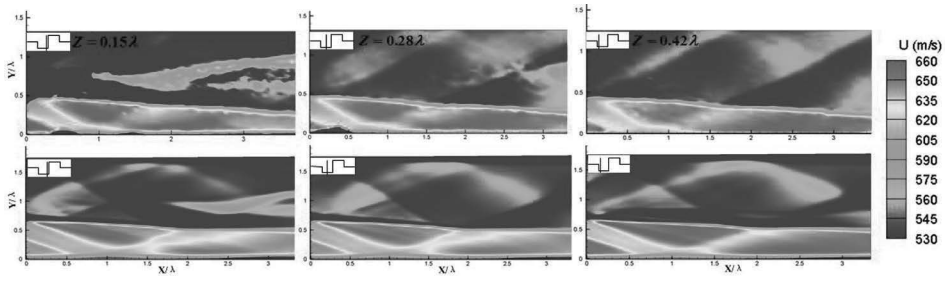


(a) Streamwise velocity

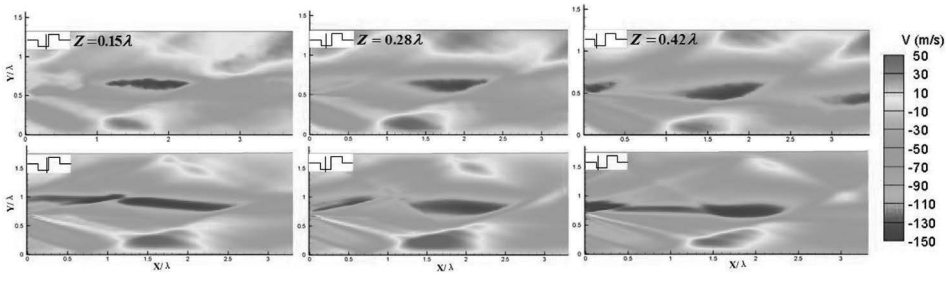


(b) Transverse velocity

Figure 6. Comparison of the velocity contours between the experimental data and the computed results with the SST $k - \omega$ model at the peak region. (a) Streamwise velocity, (b) Transverse velocity.



(a) Streamwise velocity



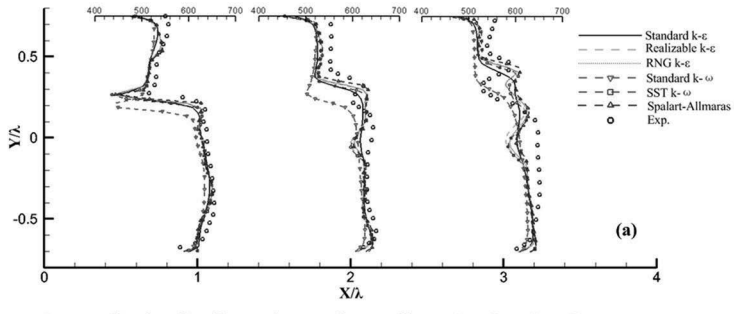
(b) Transverse velocity

Figure 7. Comparison of the velocity contours between the experimental data and the computed results with the SST $k - \omega$ model at the trough region. (a) Streamwise velocity, (b) Transverse velocity.

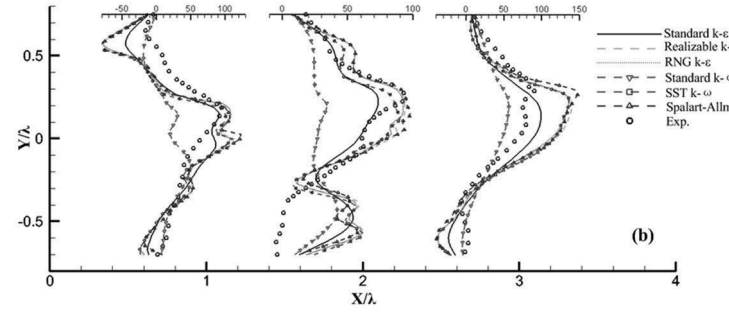
https://doi.org/10.1017/S0001924000010782 Published online by Cambridge University Press

A quantitative comparison of the averaged streamwise and transverse velocity downstream of the mixer with seven turbulent models is shown in Fig. 8. It is observed that the predictions of streamwise velocity obtained from the Realisable $k-\varepsilon$, the RNG $k-\varepsilon$, SST $k-\omega$ and Spalart-Allmaras turbulence models are very similar to each other, which show better agreement with the experimental data than that of the standard $k-\varepsilon$ and standard $k-\omega$ models. However, at the position of $X = 3\lambda$ downstream of the mixer, all of the turbulence models fail to capture accurately the streamwise velocity. A slight over prediction is observed in the mixing region. At the position of $X = \lambda$ for the averaged transverse velocity, the Realisable $k-\varepsilon$ and SST $k-\omega$ models results agree better with the experimental data than that of the others. But at the positions of $X = 2\lambda$ and $X = 3\lambda$, the averaged transverse velocity is over predicted by all of the turbulence models, while the standard $k-\omega$ model performs better compared with the others. Figure 9 shows the profiles of the averaged streamwise and transverse velocity in different X-Y planes at the streamwise position of $X = \lambda$. Similar performance of the turbulent models in predicting the flow is observed as well, with SST $k-\omega$ model being the most effective one. Furthermore, the comparison between the scalar field obtained from the SST $k-\omega$ model and that of the experiment at the different streamwise positions is provided in Fig. 10. The simulated flow structure agrees well with the NPLS images.

From the above discussion, it is obvious that none of the turbulence models investigated can predict exactly the supersonic flow field downstream of the lobed mixer. However, all the turbulence models except for the standard $k-\omega$ model show the correct tendency compared with the experimental data. The averaged streamwise and transverse velocity predicted by the SST $k-\omega$ turbulence models are in reasonable agreement with experimental data in the near field downstream



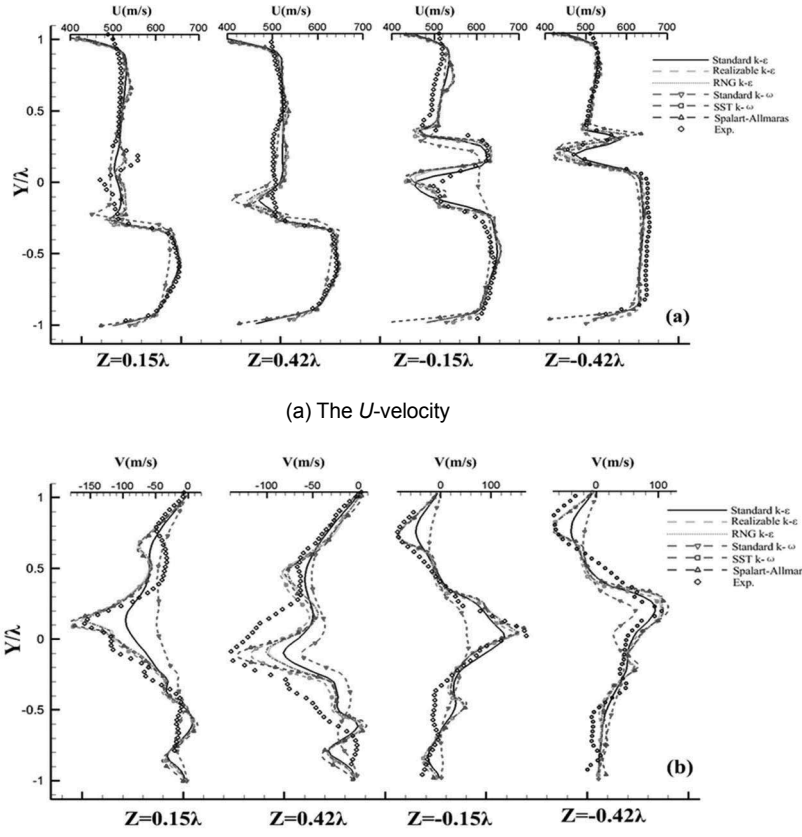
(a) The *U*-velocity



(b) The *V*-velocity

Figure 8. Comparison of streamwise and transverse velocity profiles for different turbulent models at different positions downstream of trailing edge at the measure plane of $L = -0{\cdot}28\lambda$. (a) The *U*-velocity, (b) The *V*-velocity.

https://doi.org/10.1017/S0001924000010782 Published online by Cambridge University Press



(a) The *U*-velocity

(b) The *V*-velocity

Figure 9. Comparison of streamwise and transverse velocity profiles for different turbulent models at different measure planes at downstream position of $X = \lambda$ (a) The *U*-velocity, (b) The *V*-velocity.

of the mixer but are not as good in the far field. It is now possible to explain why the turbulence models fail to predict accurately the velocity in the far field. Although these turbulence models can predict accurately the large-scale streamwise structures (see in Fig. 10), the small-scale vortical structures observed in our former experimental work[52] cannot be captured exactly by the steady RANS method with these turbulence models. Besides, it is obvious from the Figs 6, 7 and 10 that the mixing layer and the scalar interface from the calculated results are smoother than the experimental data. The small-scale turbulence structures at the mixing layer are clearly shown in the NPLS images, but not be seen in the scalar pictures obtained by the simulations in Fig. 10. Hence, in the far field, the streamwise vortices begin to break into smaller one, and the steady RANS methods with these turbulence models cannot reproduce the breakdown process and small-scale structure, which causes a poor prediction of velocities in the far field. However, the main flow features, including shock structure and large-scale streamwise vortices, can be captured exactly by the SST $k - \omega$ model.

At the same time, the supersonic mixing mechanisms of lobed mixers which are obtained by the experimental and computational approaches are analysed here. In Fig. 8, at the positions of $X = \lambda$, the sharp change of the *U*-velocity in *Y* direction smooth rapidly, which indicates the efficient

https://doi.org/10.1017/S0001924000010782 Published online by Cambridge University Press

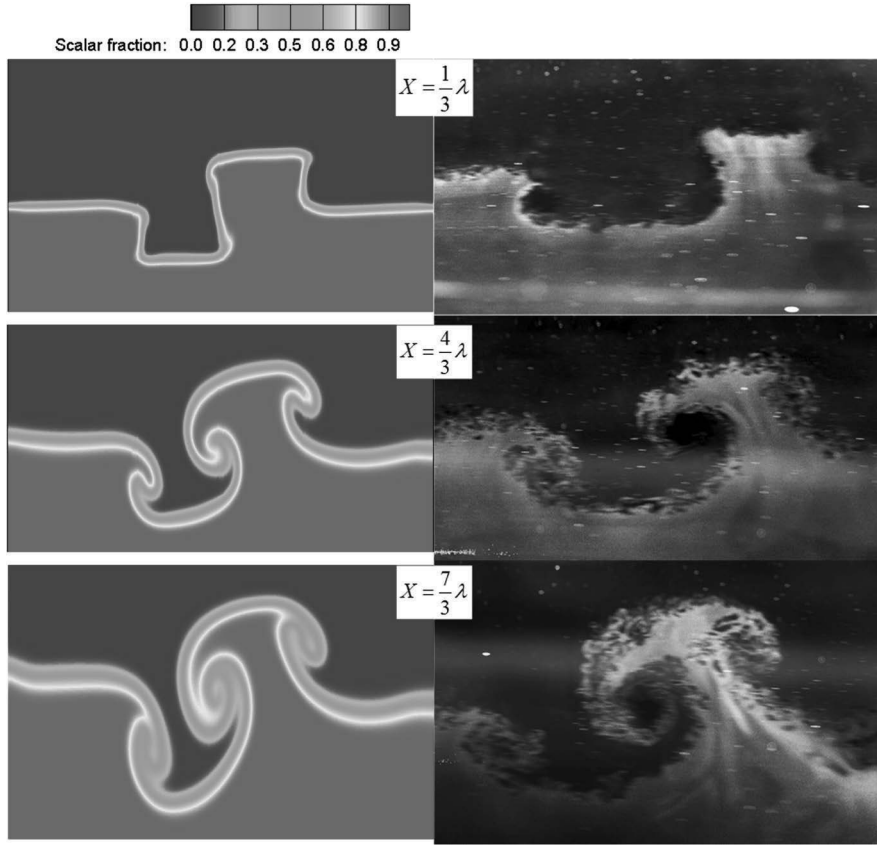


Figure 10. The cross-section scalar structures comparison between the numerical results with SST $k-\omega$ model (on the left) and the NPLS images (on the right).

mixing of the high-speed and low-speed streams. It is also observed that the V-velocity becomes greater gradually with the developing of lobed flows, which means that the cross-section secondary flow is enhanced due to the induction of streamwise vortices. Furthermore, it is noticeable that the convoluted shear layer is formed at the initial downstream of the trailing edge in Fig. 10. With the development of supersonic lobed flow, the convoluted shear layer is stretched and deformed by three large-scale counter-rotating vortical structures shed from the trailing edge, and this leads to the three streamwise vortices (see in Fig. 10). A 'pinch-off' structure proposed by the McCormick and Bennett[17] is also formed in supersonic flow because of the streamwise vortices effect, suggesting that the supersonic mixing mechanisms of lobed mixers are similar to those of incompressible regimes. That is the large-scale streamwise vortices deform the K-H vortices into a 'pinch-off' structure which is unstable and create intense turbulence, thereby inducing much earlier small-scale turbulence structures and causing the mixing enhancement. However, two points should be noted in supersonic lobed flow: one is that the streamwise vortices retain clearly at the position of downstream of mixer, as referred to the position of (see in Fig. 10), while the streamwise vortices in incompressible flow are dissipated at the station of downstream of the trailing edge[17]. It means that the supersonic streamwise vortices evolve the longer distance than the incompressible counterpart

https://doi.org/10.1017/S0001924000010782 Published online by Cambridge University Press

before their dissipation. Hence, the streamwise vortices are more effective in supersonic regime. This finding coincides with those obtained by the Tew[37] who thought reduced shear growth rate associated with high compressibility caused this behaviour. Another point is that small-scale turbulence structures which are shown clearly in the NPLS images of Fig. 10 are formed at the edge of the 'pinch-off' structure. It can be confirmed that these small-scale structures are shed by a sort of instability of the K-H vortices but not by the breakdown of the streamwise vortices. Previous studies of incompressible lobed flow indicated that there were two main instability modes for the K-H vortices in the wake of the mixer[31,46]. Herein, it is speculated that the small-scale structures are shed by the secondary K-H instability modes. Unfortunately, the numerical results obtained by the steady RANS with seven turbulence models cannot reproduce the formation process of the small-scale structure which is believed to can enhance turbulent mixing.

4.3 Impact of inflow parameters

For the investigation of planar shear layer, the important parameters affecting the growth rate of the mixer layer are the velocity ratio, the density ratio and the convective Mach number[1,53]. The velocity ratio and density ratio are the ratios of the respective properties of the inflow streams, and the convective Mach number is introduced to correlate the effect of compressibility on the growth rate of the mixing layer. The velocity ratio, the density ratio and the convective Mach number can be calculated as:

$$r = \frac{U_1}{U_2} \quad \ldots (8)$$

$$s = \frac{\rho_1}{\rho_2} \quad \ldots (9)$$

$$M_c = \frac{U_1 - U_2}{a_1 + a_2} \quad \ldots (10)$$

In present study, the influences of the velocity ratio and the convective Mach number M_c on the mixing characteristics of the lobed mixer are investigated numerically using the SST $k-\omega$ turbulence model. This model is believed to provide a good prediction on the supersonic lobed flow from the former analysis. These inflow parameters are designed by changing the total temperature or the velocity of the upper stream. The detailed information of the computational cases is exhibited in Table 2. The Case-0 also is the 'base case'. The Case-1, Case-2 and Case-3 have the same velocity ratio but different convective Mach numbers, and the convective Mach numbers of the Case-4 and Case-5 are much higher than the former cases. Besides, the characteristic Reynolds number for the lobed flow based on the mean velocity of the free-stream flows and the wavelength of the lobed mixer [30] is calculated as:

$$\mathrm{Re}_\lambda = \frac{U_a \lambda}{\nu} \quad \ldots (11)$$

Where ν is the kinematic viscosity. The characteristic Reynolds number for all the cases is tabulated in Table 2, where *tp* represents the free stream total pressure ratio of the upper to the lower streams and can be calculated as:

$$tp = \frac{P_{01}}{P_{02}} \quad \ldots (12)$$

https://doi.org/10.1017/S0001924000010782 Published online by Cambridge University Press

Where P_{01} and P_{02} denote the free stream total pressures of the upper and lower stream respectively. The influence influences of the velocity ratio, the convective Mach number and the total pressure ratio on the streamwise vorticity development and the mixing rate are investigated in following analysis.

Table 2
Information for all of the computational cases

Computational case		Ma	T_0(K)	P_0(KPa)	*tp*	*S*	U_a(ms^{-1})	M_c	Re/10^5
Case-0	Upper stream	3·3	300	101·3	1·00	1·00	646·8	0·00	2·00
	Lower stream	3·3	300	101·3					
Case-1	Upper stream	2·1	300	18·8	0·19	0·69	589·9	0·25	1·13
	Lower stream	3·3	300	101·3					
Case-2	Upper stream	3·3	205	101·3	1·00	1·46	589·9	0·32	2·70
	Lower stream	3·3	300	101·3					
Case-3	Upper stream	1·1	721	4·6	0·05	0·20	589·9	0·16	0·34
	Lower stream	3·3	300	101·3					
Case-4	Upper stream	1·0	300	3·8	0·04	0·43	485·1	0·62	0·59
	Lower stream	3·3	300	101·3					
Case-5	Upper stream	2·1	111	18·8	0·19	1·86	485·1	0·93	2·68
	Lower stream	3·3	300	101·3					

4.3.1 The influence on the streamwise vorticity development

Figure 11 shows the normalised streamwise velocity contours for all of the computational cases at the initial station downstream of the trailing edge. For all the cases, the convoluted nature of the shear layer is clearly shown. Since the boundary-layer Reynolds numbers for all of these cases differ little from each other, the merged boundary layers of the upper and lower streams downstream of the trailing edge are nearly the same. Thus, initially in the near field of the trailing edge, the dominant effect of lobed mixer is to stretches the merged boundary layers, leading to the increase of initial interfacial area. Besides, the normalised streamwise vorticity contours at the same location are illustrated in Fig. 12. The formula of the streamwise vorticity is shown as:

$$\omega_x = \frac{\lambda}{U_a}\left(\frac{\partial W}{\partial y} - \frac{\partial V}{\partial z}\right) \quad \ldots (13)$$

Here, W and V are the averaged transverse and spanwise velocities respectively, and the vorticity is normalised by U_a/λ. Positive value of the vorticity in Fig. 12 corresponds to a clockwise rotation viewed from upstream. It is revealed from the Fig. 12 that the streamwise vorticity is concentrated near the vertical parallel walls, which scales similarly to the lobe height. It is obvious that the middle vortex is the largest in scale. The similar distributions of streamwise velocity and vorticity contours for all the cases denote that the convective Mach number and the velocity ratio have a marginal influence on the generation of the streamwise vorticity. Besides, additional streamwise vorticity generated by the wake instabilities due to the thick lips of mixers can be observed in Fig. 12, whose strength mainly depends on the velocity ratio.

Further downstream, the streamwise velocity diffuses gradually, causing the rapid exchange of momentum, which contributes to the mixing enhancement. The normalised streamwise velocity

https://doi.org/10.1017/S0001924000010782 Published online by Cambridge University Press

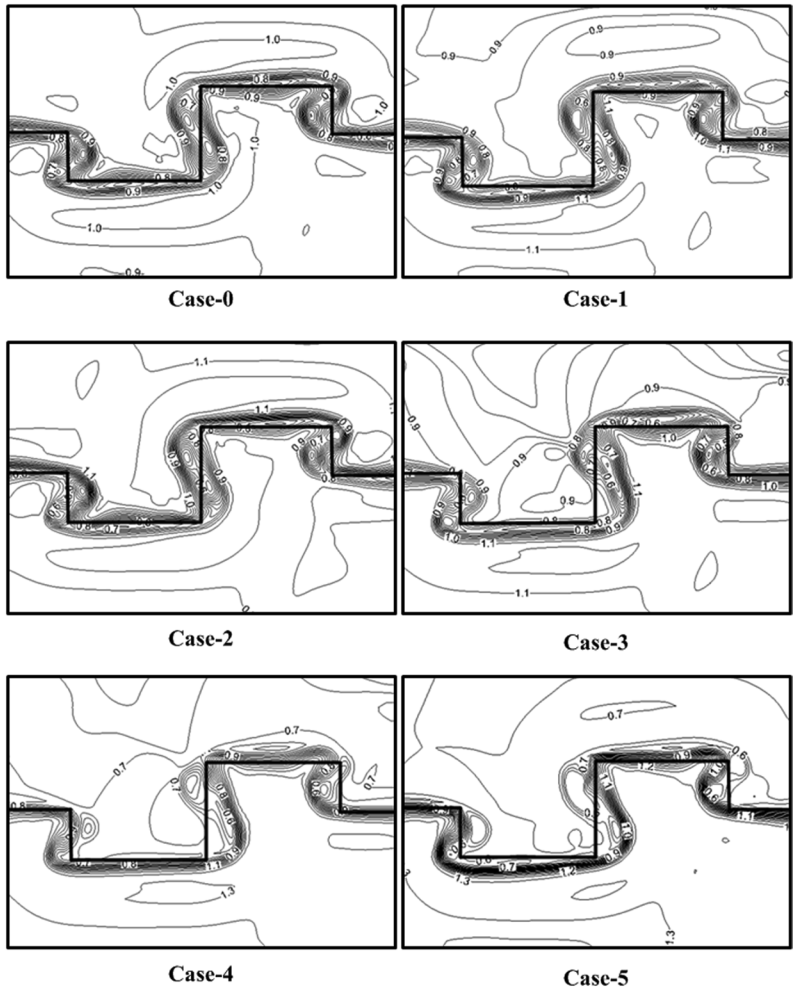


Figure 11. Contours of the normalised streamwise velocities (U/U_a) for different cases at the station of x = 0·5λ downstream of the trailing edge.

contours at the location of downstream of the trailing edge are shown in Fig. 13. A rather diffused field appears and the 'pinching-off' structure is clearly observed due to the stretching and rotation of shear layers. Another prominent feature is the higher protrusion of these structures in the upper stream region, leading to more curving shear-layer near the lobe peak compared with that near the lobe trough, which may be brought by the high-speed stream with higher momentum, making it penetrates into low-speed region more easily. In addition, there are the obvious discrepancies for the streamwise velocity contours among the six computational cases. For the Case-0, the streamwise velocity contour diffuses more fairly, but the diffused region is smaller than the other cases. For the Case-1, Case-2 and Case-3, the thicknesses of the shear layer are in simialr order of magnitude, but the penetration depths of the lobed flow drawing the lower stream to the upper region are different. It can be conjectured that this discrepancy may be caused by the convective Mach number effect

https://doi.org/10.1017/S0001924000010782 Published online by Cambridge University Press

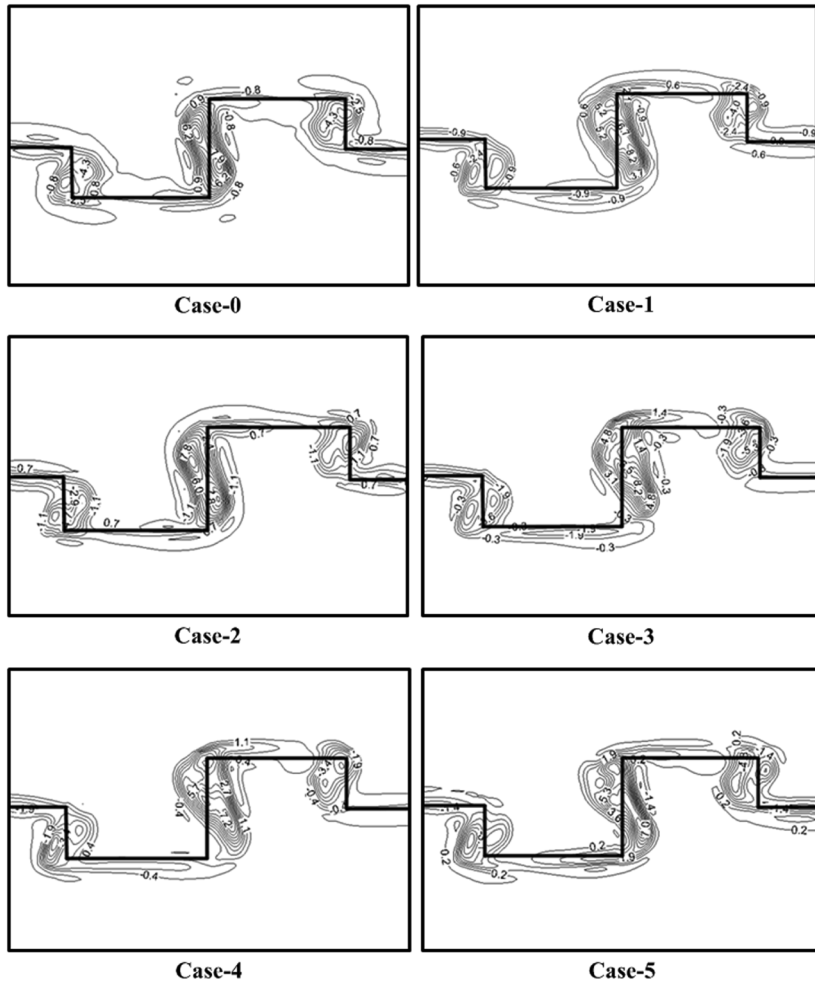


Figure 12. Contours of the normalised streamwise vorticities (ω_x) for different cases at the station of x = 0·5λ downstream of the trailing edge.

since the same velocity ratio of the three cases, and it seems that this penetration depth increases with the decreasing convective Mach number. But the similar distributions of streamwise velocity of the case-0 with convective Mach number of 0 to that of the case-3 with convective Mach number of 0·3 suggest that the penetration depth is not sensitive to the convective Mach number. Meanwhile, the effect of the density ratio and the Reynolds number on the penetration depth seems similar to that of the convective Mach number, since the streamwise vortex itself is insensitive to the compressibility and can be taken as inviscid in supersonic flow with high Reynolds number. However, as shown in Fig. 13, the penetration depth is observed to be sensitive to the total pressure ratio, which increases with the reduction of total pressure ratio. Same total pressure ratio of the case-0 and case-3 leads to similar distributions. Considering that the generation and development of streamwise vorticity is caused by the variation in aerodynamic loading along the span of the

https://doi.org/10.1017/S0001924000010782 Published online by Cambridge University Press

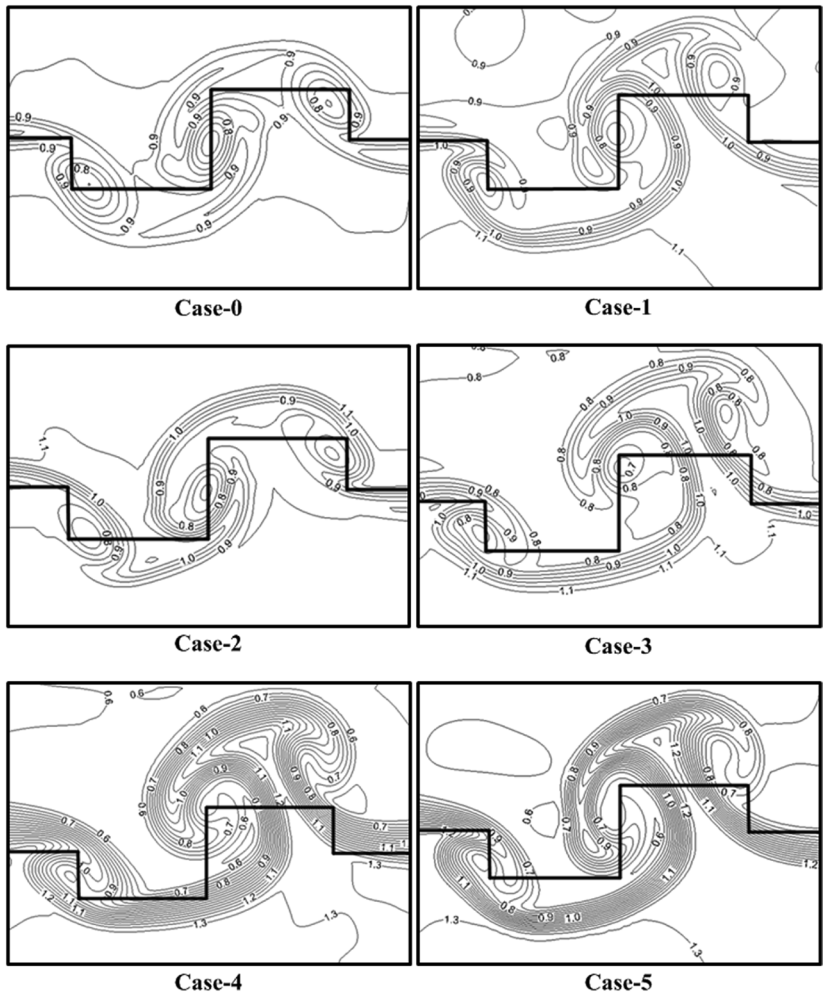


Figure 13. Contours of the normalised streamwise velocities (U/U_a) for different cases at the station of $X = 3\lambda$ downstream of the trailing edge.

mixer[35], the total pressure ratio will inevitably affect the development of streamwise vorticity. Therefore, it can be concluded that the effect of the total pressure ratio on the development of the streamwise vorticity is more significant than that of the convective Mach number.

For the Case-4 and Case-5, the lobed flow is more diffused due to the higher velocity ratio. The rolling-up mechanism of the mixing layer is analogous to that of the former cases. However, the scales of these streamwise vorticities are larger than those of the former cases, suggesting that the streamwise vorticities are affected obviously by the velocity ratio. Meanwhile, the penetration depth for the Case-4 is larger than that of the Case-5 due to the smaller total pressure ratio for the Case-4. Therefore, it is summarised that the generation of the streamwise vorticities mostly depends on the special lobed splitter plate. However, the evolution of streamwise vorticities is affected by the velocity ratio and the total pressure ratio. It is also obvious that the streamwise vorticity diffuse more rapidly with decreasing velocity ratio and total pressure ratio, which corresponds

https://doi.org/10.1017/S0001924000010782 Published online by Cambridge University Press

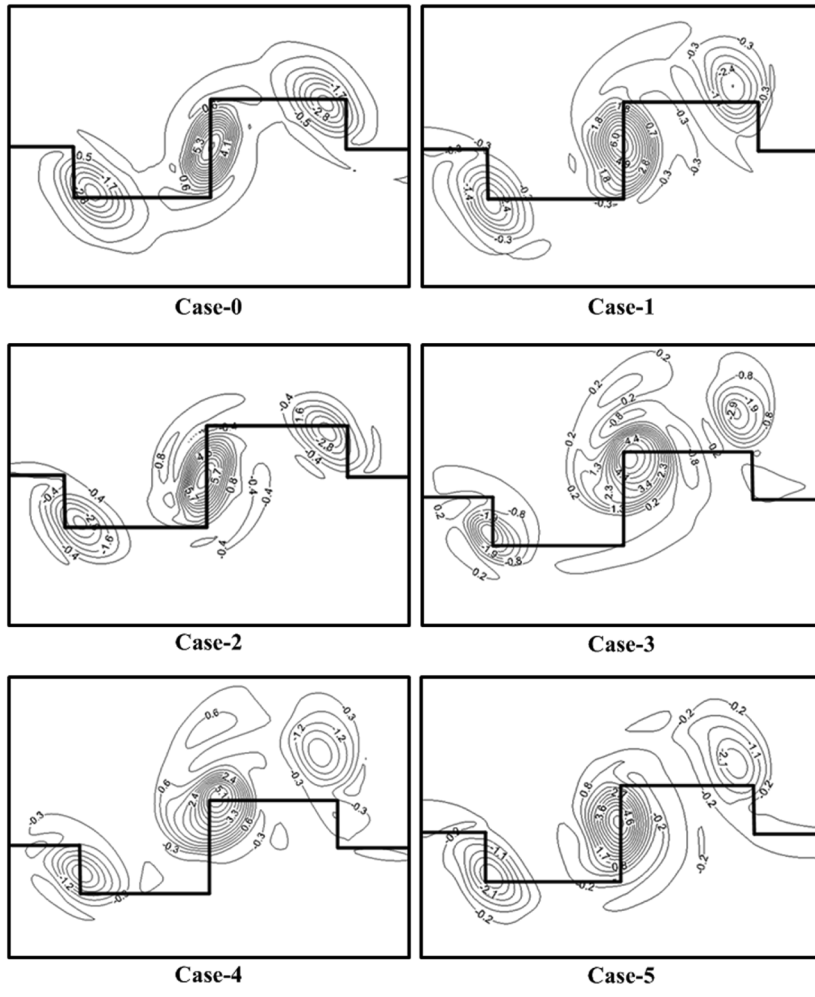


Figure 14. Contours of the normalised streamwise vorticities (ω_x) for different cases at the station of $X = 3\lambda$ downstream of the trailing edge.

to increasing velocity and total pressure difference between the upper and lower streams. The streamwise vorticity development is observed to be insensitive to the convective Mach numbers. The normalised streamwise vorticity contours shown in Fig. 14 further confirms these conclusions.

Figure 15 shows the variation of the maximum value of the streamwise vorticity with downstream distance for the calculated cases. It could be observed that the variation trends for all the cases are almost same, and their maximum values fall off with downstream distance. A steep fall happened with the initial 0·5 wavelength downstream of the trailing edge, suggesting the streamwise vorticities decay rapidly at the initial distance from the trailing edge. Farther downstream, the decay rates for all the cases tend to level off. But the initial maximum values for the Case-4 and Case-5 are larger than those of the other cases due to the enhanced streamwise vorticity brought by the wake effect of thick lips. Besides, it is observed that the profiles collapse more rapidly with the decreasing velocity ratio and total pressure ratio. These results further prove the above conclusions.

https://doi.org/10.1017/S0001924000010782 Published online by Cambridge University Press

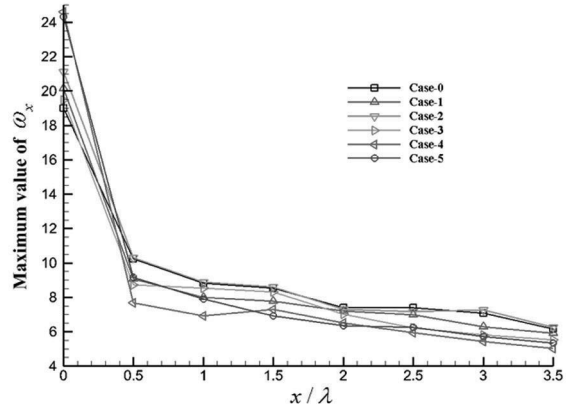


Figure 15. Variation of the maximum value of streamwise vorticities with downstream distance for all the computational cases.

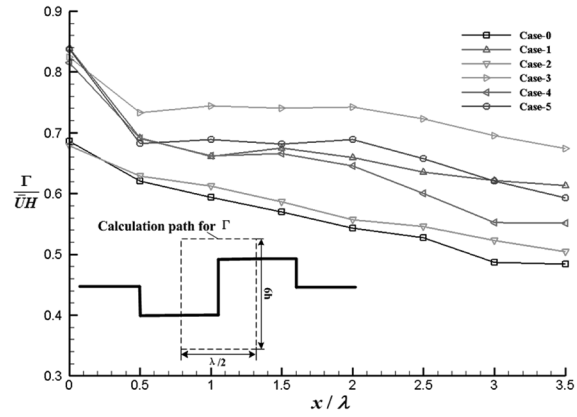


Figure16. Variation of the streamwise circulation with downstream distance for all the computational cases.

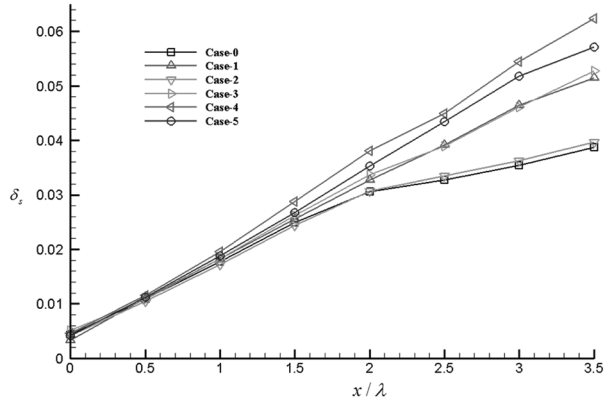


Figure 17. Variation of the scalar thickness with downstream distance for all the computational cases.

https://doi.org/10.1017/S0001924000010782 Published online by Cambridge University Press

The strength of the streamwise vorticity could be evaluated by employing the shed streamwise circulation. It is an important parameter to quantify the effectiveness of mixer characteristics, and the definition is given by:

$$\Gamma = \int_C u \cdot \mathrm{d}s = \iint_A \omega \cdot \mathrm{d}A \qquad \ldots (14)$$

The streamwise circulation is evaluated around an integration path that encompasses a region with one half-lobe and a spanwise dimension of 6*h* (see in Fig. 16). The initial streamwise circulation may be estimated by the scaling law developed by Barber *et al*[54].

$$\Gamma = 2C\bar{U}H \ \mathrm{Tan}\,\alpha \qquad \ldots (15)$$

Here, $H = 2h$ and the value of the constant C can be taken as unity for mixers with vertical side walls. Hence, the normalised streamwise circulation can be written as:

$$\Gamma^* = \frac{\Gamma}{\bar{U}H} \approx 2\,\mathrm{Tan}\,\alpha \qquad \ldots (16)$$

Using the Equation (16), the estimated non-dimensional circulations for the 15º mixer are 0·54. Fig. 16 shows the decay tendency of the normalised streamwise circulation with downstream distance. It is observed that the predicted circulations for all the cases close to the trailing edge are higher than that of the scaling law of Barber[54], since the scaling law of Barber is inadequate for the supersonic lobed flow. As seen in Fig. 16, a rapid decay of the circulations appears in a short distance downstream of the trailing edge, followed by a slight increase except for the Case-0 and Case-2. Further downstream, the decay of streamwise circulations slower for all the cases. The observed behaviour of circulation of the streamwise vortex is consistent with the results obtained by Salman, *et al*[41]. Though the velocity ratio has little influence on the generation of the circulation, the decay of circulation is obviously affected by the velocity ratio. A more rapid decay of circulation occurs with the decrease of velocity ratio. The total pressure ratio also affects the decay of the streamwise circulations. It is noticeable that the influence of the velocity ratio and total pressure ratio on the streamwise vorticity development results is responsible for this.

4.3.2 The influence on the mixing rate of lobed mixer in supersonic regimes

The streamwise vortices are an important factor to mixing enhancement for the supersonic lobed flow. Thus, the velocity ratio and the total pressure ratio should have a magnitude influence on the mixing rate of lobed mixer due to their effect on the streamwise vorticity development. However, the lack of the available assessment of mixing rate in supersonic lobed flow causes the difficulty to quantify the mixing efficiency of lobed mixer. Herein, a conception of scalar thickness that commonly exists in the realm of mixing layer[55] is adopted to reflect the mixing rate of lobed mixer, and it is defined as an averaged integral over an area that encompasses a region with a spanwise dimension of 1·6λ and a height of 8*h*. This is given by:

$$\delta_s = \frac{1}{A_{yz}} \int_{-0{\cdot}8\lambda}^{0{\cdot}8\lambda} \int_{-4h}^{4h} Y_f (1 - Y_f)\, \mathrm{d}y\, \mathrm{d}z \qquad \ldots (17)$$

Here, T_f is the mass fraction of the component of the mixture; A_{ys} is the area that encompasses the integral region. The scalar thickness with downstream distance for all the cases is provided in

https://doi.org/10.1017/S0001924000010782 Published online by Cambridge University Press

Fig. 17. It is clear that the scalar thickness for all the cases increases when moving downstream since the scalar interfacial area of two streams increases for the stretching of the streamwise vortices[37], which indicates that the lobed mixer is also effective in supersonic flow in mixing enhancement. At the same time, it is observed that the growth rate for all the cases within one wavelength downstream of the trailing edge is almost same, but further downstream, the deviations among these cases gradually expand. The Case-4 has the largest scalar thickness, and followed by the Case-5. Conversely, the smallest thickness belongs to the Case-0, and the Case-2 is extremely close to the Case-0. The scalar thickness for the Case-1 and Case-3 is almost same and lies in the middle level. Hence, this suggests that the velocity ratio has an apparent influence on the mixing characteristic of the lobed mixer, and the smaller velocity ratio leads to the better mixing characteristic of mixer. In addition, the total pressure ratio also affects the mixing rate of lobed mixer. This result is consistent with the former findings regarding the streamwise vorticity and the related circulation.

5.0 CONCLUSION

A detailed study on the characteristics of the supersonic flow in the near field of a lobed mixer is conducted both experimentally and numerically. The velocity vector and scalar fields of the streamwise and transverse measured planes are obtained using the PIV and NPLS techniques. A steady RANS method is employed, and the effectiveness of the turbulence model as well as the influence of the inflow parameters on the mixing characteristics of the lobed mixer is studied numerically. Some conclusions are drawn as follows:

(1) In spite of the difficulties in accurately predicting the three-dimensional turbulent field downstream of the lobed mixer, the averaged velocity and scalar quantities and their trend of development are in reasonable agreement with the experimental data. The SST turbulence models is more effective in predicting the main flow features including shock waves and streamwise vortices downstream of lobed mixer.

(2) The K-H vortices are stretched and rotated by the large-scale streamwise vortices that shed from the vertical walls of the mixer's trailing edge, leading to the formation of an unstable 'pinching-off' structure, while the streamwise vortices maintain in a long distance preserving the initial rotations and bringing more effective mixing.

(3) The generation of streamwise vorticity mainly depends on the configuration of the lobed mixer. The evolution of streamwise vorticity is affected obviously by the velocity ratio, and higher velocity ratio leads to higher decay rate of streamwise vorticity. In addition, the streamwise vorticity is more sensitive to the total pressure ratio than to the convective Mach number. With the decrease of the total pressure ratio, the streamwise vorticity decays more rapidly. The convective Mach number can be believed to have a marginal effect on the streamwise vorticity development.

(4) The scalar thickness which reflects the mixing performance of the lobed mixer is affected by the velocity ratio and the total pressure ratio. The scalar thickness increases with the decrease of velocity ratio and total pressure ratio, which means that this thickness increases with the increasing free-stream velocity and total pressure difference. The velocity ratio and the total pressure ratio affect the streamwise vorticity development, and then have an effect on the mixing rate of the lobed mixer.

https://doi.org/10.1017/S0001924000010782 Published online by Cambridge University Press

ACKNOWLEDGEMENT

This work has been supported by the National Natural Science Foundation of China (Grant No. 11272351).

REFERENCES

1. PAPAMOUSCHOU, D. and ROSHKO, A. The compressible turbulent shear layer: An experimental study, *J Fluid Mechanics*, 1988, **197**, pp 453-477.
2. ELLIOTT, G.S. and SAMIMY, M. Compressibility effects in free shear layers, *Physics of Fluids*, 1990, **A2**, pp 1231-1240.
3. GUTMARK, E.J., SCHADOW, K.C. and YU, K.H. Mixing enhancement in supersonic free shear flows, *Annu Rev Fluid Mech*, 1995, **27**, pp 375-417.
4. SEINER, J.M., DASH, S.M. and KENZAKOWSKI, D.C. Historical survey on enhanced mixing in scramjet engine, *J Propulsion and Power*, 2001, **17**, (6), pp 1273-1286.
5. KUCHAR, A.P. and CHAMBERLIN, R. Scale model performance test investigation of exhaust system mixers for an energy efficient engine (E3), AIAA No 80-0229, 1980.
6. KOZLOWSKI, H. and KRAFT, H. Experimental evaluation of exhaust mixers for an energy efficient engine, AIAA No 80-1088, 1980.
7. PATERSON, R.W. Turbofan forced mixer-nozzle internal flow field, Part 1-A benchmark experimental study, NASA CR-3492, 1982.
8. GARRISON, L.A., LYRINTZIS, A.S. and BLAISDELL, G.A. RANS-Base noise predictions of jets with internal forced mixers, AIAA No 2006-2599, 2006.
9. PRESZ, W.M., Jr., REYNOLDS, G. and MCCORMICK, D. Thrust augmentation using mixer-ejector-diffuser systems, AIAA No 94-0020, 1994.
10. TILLMAN, T.G. and PRESZ, Jr., Thrust characteristics of a supersonic mixer ejector, *J Propulsion and Power*, 1995, **11**, (5), pp 931-937.
11. SHAN, Y. and ZHANG, J.Z. Numerical investigation of flow mixture enhancement and infrared radiation shield by lobed forced mixer, *Applied Thermal Engineering*, 2009, **29**, pp 3687-3695.
12. SRIKRISHNAN, A.R., KURIAN, J. and SRIRAMULU, V. Experimental study on mixing enhancement by petal nozzle in supersonic flow, *J Propulsion and Power*, 1996, **12**, (1), pp 165-169.
13. NARAYANAN, A.K. and DAMODARAN, K.A. Experimental studies on piloted supersonic combustion using the petal nozzle, *J Propulsion and Power*, 1997, **13**, (1), pp 142-149.
14. SMITH, L.L., MAJAMAK, A.J. and LAM, I.T., *et al* Mixing enhancement in a lobed injector, *Physics of Fluids*, 1997, **9**, (3), pp 667-678.
15. MAJAMAKI, A.J., SMITH, O.I. and KARAGOZIAN, A.R. Passive mixing control via lobed injectors in high-speed flow, *AIAA J*, 2003, **41**, (4), pp 623-632.
16. GERLINGER, P., STOLL, P. and KINDLER, M., *et al* Investigation of mixing and combustion enhancement in supersonic combustors by strut induced streamwise vorticity, *Aerosp Sci Technol*, 2008, **12**, pp 159-168.
17. MCCORMICK, D.C. and BENNETT, J.C. Vortical and turbulent structure of a lobed mixer free-shear layer, *AIAA J*, 1994, **3**, (29), pp 1852-1859.
18. WINANT, C.D. and BROWAND, F.K. Vortex Pairing: The mechanism of turbulent mixing-layer growth at moderate Reynolds number, *J Fluid Mechanics*, 1974, **6**, (32), pp 237–255.
19. MANNING, T.A. Experimental studies if mixing flows with streamwise vorticity, MS Thesis, Massachusetts Institute of Technology, Cambridge, 1991.
20. PATERSON, R.W. Turbofan mixer nozzle flow field-a benchmark experimental study, *ASME J of Engineering for Gas Turbines and Power*, 1984, **106**, pp 692-698.
21. WERLE, W.A., PATERSON, R.W. and PRESZ, W.M. Jr. Flow structure in a periodic axial vortex array, AIAA No 87-610, 1987.
22. ECKERLE, W.A., SHEIBANI, H. and AWAD, J. Experimental measurement of the vortex development downstream of a lobed forced mixer, *J Engineering for Gas Turbine and Power*, 1992, **114**, pp 63-71.
23. ELLIOTT, J.K., MANNING, T.A. and QIU, Y.J., *et al* Computational and experimental studies of flow in multi-lobed forced mixers, AIAA No 92-3568, 1992.
24. BELOVICH, V.M. and SAMIMY, M. Mixing processes in a coaxial geometry with a central lobed mixer-nozzle, Aerospace Sciences Meeting and Exhibit, 34th, Reno, Nevada, USA, January 1996, pp 15-18.

https://doi.org/10.1017/S0001924000010782 Published online by Cambridge University Press

25. HUI, H., TETSUO, S. and TOSHIO, K., *et al* Research on the vortical and turbulent structures in the lobed jet flow using laser induced fluorescence and particle image velocimetry techniques, *Meas Sci Technol*, 2000, **11**, pp 698-711.
26. HUI, H., TETSUO, S. and TOSHIO, K., *et al* A study on a lobed jet mixing flow by using stereoscopic particle image velocimetry technique, *Physics of Fluids*, 2001, **13**, pp 3425-3441, 2001.
27. HUI, H., TETSUO, S. and TOSHIO, K., *et al* Mixing process in a lobed jet flow, *AIAA J*, 2002, **40**, (7), pp 1339-1345.
28. HUI, H., TETSUO, S. and TOSHIO, K., *et al* Simultaneous measurements of all three components of velocity and vorticity vectors in a lobed jet flow by means of dual-plane stereoscopic particle image velocimetry, *Physics of Fluids*, 2002, **14**, pp 2128-2138.
29. YU, S.C.M. and XU, X.G. Confined coaxial nozzle flow with central lobed mixer at different velocity ratios, *AIAA J*, 1998, **36**, (3), pp 349-358.
30. MAO, R.H., YU, S.C.M. and CHUA, L.P. Kelvin-Helmholtz and streamwise vortices in the near wake of a single-lobe forced mixer, Proceedings of the institution of mechanical engineers, *Part G: J Aerospace Engineering*, 2006, **220**, pp 279-298.
31. MAO, R H., YU, S.C.M and ZHOU, T., *et al* On the vorticity characteristics of lobe-forced mixer at different configurations, *Exp. Fluids*, 2009, **46**, pp 1049-1066.
32. NASTASE, I., MESLEM, A. and GERVAIS, P. Primary and secondary vortical structures contribution in the entrainment of low Reynolds number jet flows, *Exp Fluids letter*, 2008, **44**, pp 1027-1033.
33. NASTASE, I. and MESLEM, A. Vortex dynamics and mass entrainment in turbulent lobed jets with and without lobe deflection angles, *Exp Fluids*, 2010, **48**, pp 693-714.
34. HASSAN, M.E. and MESLEM, A. Time-resolved stereoscppic particle image velocimetry investigation of the entrainment in the near field of circular and daisy-shaped orifice jets, *Physics of Fluids*, 2010, **22**, pp 1-26.
35. WAITZ, I.A., QIU, Y.J. and MANNING, T.A. Enhanced mixing with streamwise vorticity, *Prog Aerospace Sci*, 1997, **33**, pp 323-351.
36. TEW, D.E. Streamwise vorticity enhanced compressible mixing downstream of lobed mixers, Doctor's thesis, Massachusetts Institute of Technology, Cambridge, 1997.
37. TEW, D.E. and WAITZ, I.A. Impact of compressibility on mixing downstream of lobed mixers, *AIAA J Technical notes*, 2002, **42**, (11), pp 2393-2396.
38. KOUTMOS, P. and MCGUIRK, J.J. Turbofan forced mixer/nozzle temperature and flow field modeling, *International J Heat and Mass Transfer*, 1989, **32**, (6), pp 1141-1153.
39. O'SULLIVAN, M.N., WAITZ, I. A. and GREITZER, E.M., *et al* A Computational study of viscous effects on lobed mixer flow features and performance, AIAA No 94-3085, 1994.
40. SALMAN, H., MCGUIRK, J.J. and PAGE, G.J. A numerical study of vortex interactions in lobed mixer flow fields, AIAA No 99-33596, 1999.
41. SALMAN, H., PAGE, G.J. and MCGUIRK, J.J. Prediction of lobed mixer vortical structures with a turbulence model, *AIAA J*, 2003, **41**, (5), pp 878-887.
42. GEORGIADIS, N.J., RUMSEY, C.L. and YODER, D.A., *et al* Turbulence modeling effects on calculation of lobed nozzle flowfields, *J Propulsion and Power*, 2006, **22**, (3), pp 567-576.
43. STRICKLAND, J.H., SELERLAND, T. and KARAGOZIAN, A.R. Numerical simulations of a lobed fuel injector, *Physics of Fluids*, 1998, **10**, (11), pp 2950-2964.
44. OOBA, Y., KODAMA, H. and NAKAMURA, Y., *et al* Large eddy simulation analysis of a 18-lobe convoluted mixer nozzle, AIAA No 2002-0717, 2002.
45. BEBONIS, J.R. Progress toward large-eddy simulations for prediction of realistic nozzle systems, *J Propulsion and Power*, 2007, **23**, (5), pp 971-980.
46. BRINKERHOFF, J.R., ORIA, H. and YARAS, M.I. Experimental and computational study of mixing mechanisms in an axisymmetric lobed mixer, *J Propulsion and Power*, 2013, **29**, (5), pp 1017-1030.
47. ZHAO, Y.X., YI, S.H. and TIAN, L.F., *et al* Supersonic flow imaging via nanoparticles, *Science in China Series E: Technological Sciences*, 2009, **52**, pp 3640-3648.
48. WANG, D.P., ZHAO, Y.X. and XIA, Z.X., *et al* Experimental investigation of supersonic flow over a hemisphere, *Chinese Science Bulletin Fluid Mechanics*, 2012, **57**, (15), pp 1765-1771.
49. WANG, B., LIU, W.D. and ZHAO, Y.X., *et al* Experimental investigation of the micro-ramp based shock wave and turbulent boundary layer interaction control, *Physics of Fluids*, 2012, **24**, pp 617-630.
50. WANG, D.P., XIA, Z.X. and ZHAO, Y.X., *et al* Vortical structures of supersonic flow over a delta-wing on a flat plate, *Applied Physics Letters*, 2013, **102**, pp 1-4.
51. Fluent Inc Fluent 6.3 User's Guide, Fluent Inc., Lebanon, New Hampshire, USA, 2006.

https://doi.org/10.1017/S0001924000010782 Published online by Cambridge University Press

52. WANG, Q.H., WANG, Z.G. and LEI, J. *et al* Characteristics of mixing enhanced by streamwise vortices in supersonic flow, *Applied Physics Letters*, 2013, **103**, pp 1-4.
53. BROWN, G. and ROSHKO, A. On density effects and large structures in turbulent mixing layers, *J Fluid Mechanics*, 1974, **64**, pp 775-816.
54. BARBER, T., PATERSON, R.W. and SKEBE, S.A. Turbofan forced mixer lobe flow modeling, Technical Report CR-4147 NASA, 1988.
55. CARLOS, P.R. Compressibility effects in turbulent nonpremixed reacting shear flows, Doctor Thesis, Mechanical Engineering, University of California, San Diego, USA, 2000.

https://doi.org/10.1017/S0001924000010782 Published online by Cambridge University Press